NANO LETTERS

Letter

pubs.acs.org/NanoLett

Revealing Nanoscale Passivation and Corrosion Mechanisms of Reactive Battery Materials in Gas Environments

Yuzhang Li,[†,⊥] Yanbin Li,[†,⊥] Yongming Sun,[†] Benjamin Butz,[†,‡] Kai Yan,[†] Ai Leen Koh,[§] Jie Zhao,[†] Allen Pei,[†] and Yi Cui*[,†,∥]

[†]Department of Materials Science and Engineering, Stanford University, Stanford, California 94305, United States

[‡]Institut für Mikro- und Nanostrukturforschung, Friedrich-Alexander-Universität Erlangen-Nürnberg, Cauerstrasse 6, 91058 Erlangen, Germany

[§]Stanford Nano Shared Facilities, Stanford University, Stanford, California 94305, United States

[∥]Stanford Institute for Materials and Energy Sciences, SLAC National Accelerator Laboratory, 2575 Sand Hill Road, Menlo Park, California 94025, United States

Supporting Information

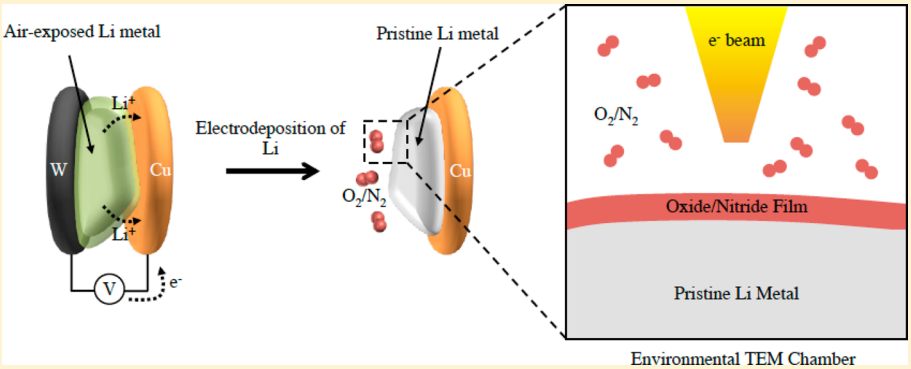

ABSTRACT: Lithium (Li) metal is a high-capacity anode material (3860 mAh g^{-1}) that can enable high-energy batteries for electric vehicles and grid-storage applications. However, Li metal is highly reactive and repeatedly consumed when exposed to liquid electrolyte (during battery operation) or the ambient environment (throughout battery manufacturing). Studying these corrosion reactions on the nanoscale is especially difficult due to the high chemical reactivity of both Li metal and its surface corrosion films. Here, we directly generate pure Li metal inside an environmental transmission electron microscope (TEM), revealing the nanoscale passivation and corrosion process of Li metal in oxygen (O_2), nitrogen (N_2), and water vapor (H_2O). We find that while dry O_2 and N_2 (99.9999 vol %) form uniform passivation layers on Li, trace water vapor (~1 mol %) disrupts this passivation and forms a porous film on Li metal that allows gas to penetrate and continuously react with Li. To exploit the self-passivating behavior of Li in dry conditions, we introduce a simple dry-N_2 pretreatment of Li metal to form a protective layer of Li nitride prior to battery assembly. The fast ionic conductivity and stable interface of Li nitride results in improved battery performance with dendrite-free cycling and low voltage hysteresis. Our work reveals the detailed process of Li metal passivation/corrosion and demonstrates how this mechanistic insight can guide engineering solutions for Li metal batteries.

KEYWORDS: *In situ TEM, lithium metal battery, environmental TEM, passivation, corrosion*

The development of advanced materials for renewable energy generation and storage is crucial for creating a sustainable future.[1] New breakthroughs depend on an intimate understanding of such materials. Real-time probing of chemical and electrochemical reactions using X-ray and electron microscopy/spectroscopy have given us unprecedented knowledge into the nanoscale working mechanisms of batteries,[2−6] catalysts,[7,8] and nanocrystal syntheses,[9,10] providing tremendous insight for designing potential improvements. These exciting examples highlight the necessity of both real-time and real-environment monitoring of relevant phenomena during operating conditions (operando). New challenges emerge when materials of interest have high chemical reactivity. For example, Li metal easily tarnishes in ambient air,[11,12] which would affect operando TEM observations of the sensitive material depending on its previous environmental exposure. Studying these reactive materials requires generating a pure sample without prior history of exposure to outside environments and subsequent observation of their chemical and electrochemical reactions under the environment of interest. Here, we demonstrate this important capability by direct electro-

Received: June 21, 2017
Published: July 10, 2017

DOI: 10.1021/acs.nanolett.7b02630
Nano Lett. XXXX, XXX, XXX−XXX

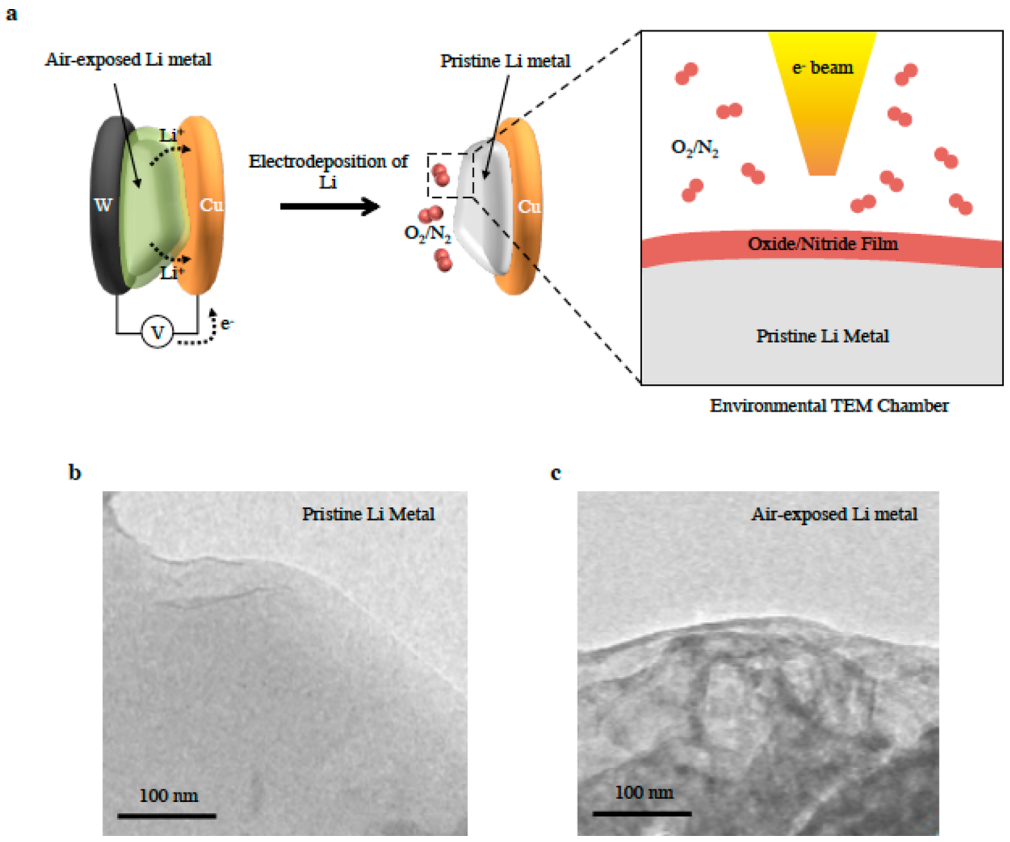

Figure 1. Li metal deposition inside environmental TEM. (a) Schematic of the Li deposition process using an electrical biasing TEM holder. Li metal exposed briefly (~3 s) in air during transfer into the TEM column forms oxides and nitrides that serve as a solid electrolyte to conduct Li ions. Upon applying a voltage bias, Li metal is deposited onto the copper substrate. With a clean and pristine surface, the deposited Li metal is then exposed to dry and wet O_2 or N_2. (b) TEM image of the pristine Li metal surface necessary for meaningful studies of the initial reaction between Li and gas. (c) TEM image of Li metal exposed to the ambient air. The corrosion products formed on the Li surface interfere with its reactions with gas.

deposition of Li metal inside a high-vacuum environmental TEM chamber, followed by exposure to key gaseous species for operando observation.

Widely considered to be the holy grail of battery research, Li metal has the highest specific capacity (3860 mAh g^{-1}) and lowest electrochemical potential of all anodes, making it a promising candidate to enable high-energy batteries for portable electronics, electrical vehicles, and grid-scale energy storage.[13,14] However, Li metal is highly reactive, which drives the electrochemical decomposition of organic liquid electrolyte during battery operation.[15,16] This process consumes Li salts and electrolyte to form a fragile solid electrolyte interphase (SEI) on the Li metal surface. The SEI is then repeatedly broken and reformed due to Li metal's infinite volume change and dendritic growth[17] that is intrinsic to its electrochemical deposition and stripping during battery charge and discharge, respectively. Furthermore, these failure modes would be exacerbated by Li metal's side reactions with the environment throughout a realistic manufacturing process occurring outside of an inert atmosphere. As a result, low Coulombic efficiencies, poor cycle life, and safety concerns caused by continuous electrolyte consumption and dendrite growth preclude Li metal from being a practical anode material. Recently, there has been significant interest and effort to address these problems with some success.[18−28] However, the overwhelming emphasis of both fundamental studies and engineering approaches has been toward materials that are assumed to be pristine once assembled into batteries; previous environmental exposure and its effects on battery performance are largely neglected. Li metal foil, a common form of Li used in batteries, is often exposed to a gaseous environment after it is made. Li metal's high chemical reactivity implies that a past history of environmental exposure could adversely affect its electrochemical behavior in battery cells.[29−31] Therefore, understanding the initial reaction between a pristine Li metal surface with the surrounding environment would be essential for guiding practical battery designs in the future.

For reactive materials, especially on the nanoscale, operando TEM studies of corrosion reactions are difficult. Before any observation can occur, the sample spontaneously forms a surface corrosion film due to brief environmental exposure, affecting its interaction with gases later introduced into the system. Previous studies of Li metal corrosion were thus limited to measuring the increase in sample mass over time and optically detecting surface changes as Li metal was continuously exposed to various gases.[11,12] While useful, these macroscopic studies cannot properly explain the relevant phenomena happening at the nanoscale. At present, direct observation of the Li metal reaction with relevant gaseous species (e.g., O_2, N_2, H_2O) and a clear understanding of this passivation/corrosion process remain absent. Our work here is to fill this knowledge gap.

Generating Pristine Li Metal Directly Inside the TEM. Since any meaningful gas study requires a pristine and clean Li metal surface, Li metal must be generated inside a controlled environment within the TEM. Using an electrical biasing TEM

DOI: 10.1021/acs.nanolett.7b02630
Nano Lett. XXXX, XXX, XXX−XXX

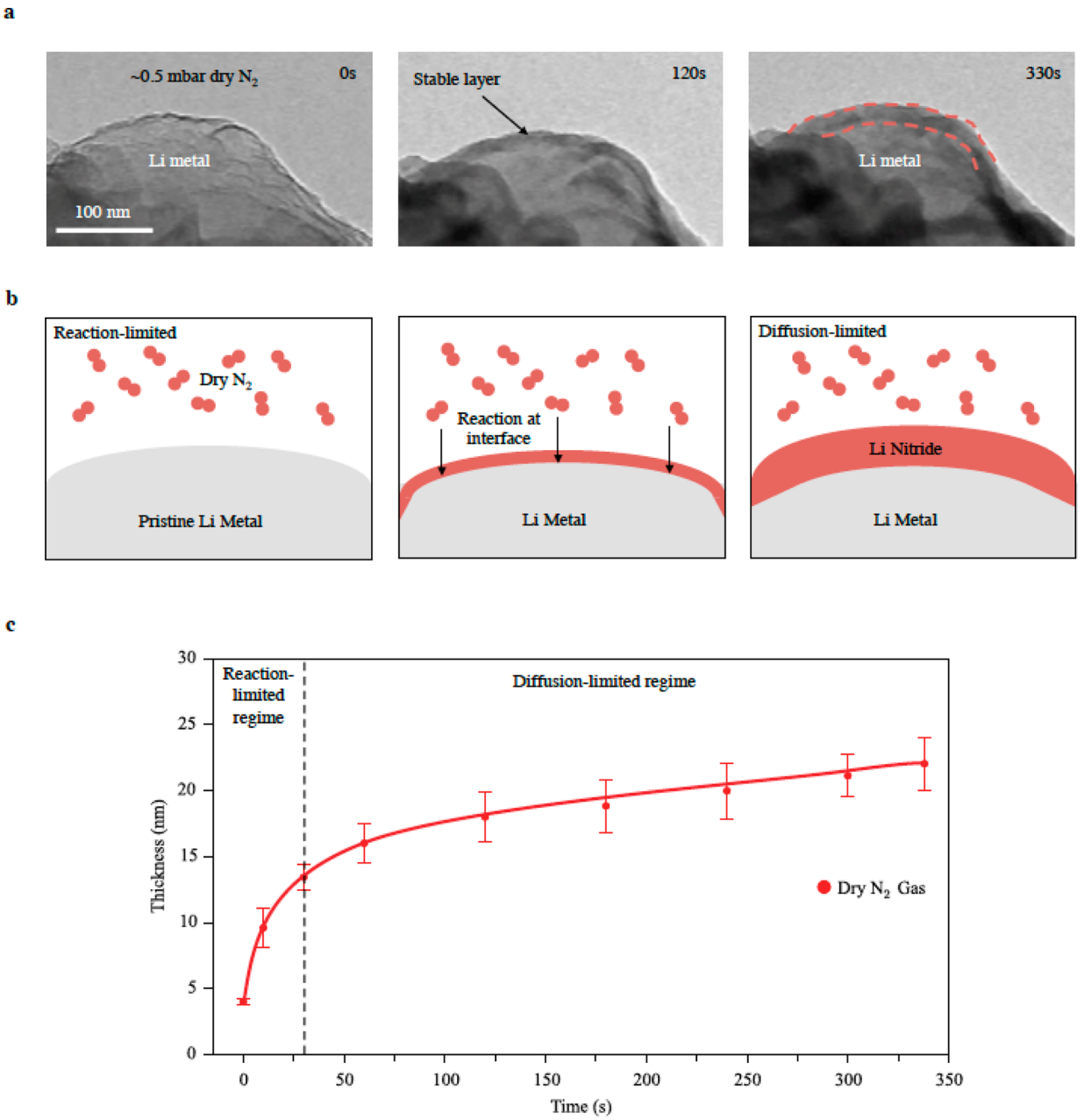

Figure 2. Passivation reaction of Li metal in dry N_2 gas. (a) Time-lapse TEM images of Li metal reacting with dry N_2 taken from Movie S1, Supporting Information. A smooth and uniform passivation layer (outlined by dashed red lines) forms on the Li metal surface, preserving its original morphology. (b) Schematic illustrating the passivation mechanism of Li metal in dry N_2. The reaction is localized at the interface between Li metal and N_2 gas. (c) Graph of passivation layer thickness measured over time. Two growth modes are identified: a reaction-limited regime at early times (left of dashed line) and a diffusion-limited regime at later times (right of dashed line). Guides for the eye are provided as lines through the data points.

holder, we deposit bare Li metal onto a copper substrate while under high vacuum (~10^{-7} mbar) inside the TEM column (Figure 1a). Following deposition, the Li metal surface is clean without any corrosion film formed from previous exposure (Figure 1b). In contrast, Li metal that is exposed briefly to air (~3 s) during transfer from an inert atmosphere into the TEM quickly forms surface corrosion products (Figure 1c). To monitor the reaction between fresh Li metal and relevant gases in real time, we introduce "dry" (99.9999 vol % purity) or "wet" (~1 mol % H_2O content) O_2 and N_2 inside the environmental TEM at ~0.5 mbar. Chemical analysis by electron energy loss spectroscopy (EELS), energy-filtered transmission electron microscopy (EFTEM), and selected area electron diffraction (SAED) allows us to identify the gas-formed corrosion products. By generating pristine Li metal directly in an environmental TEM, we can elucidate its passivation process when exposed to dry O_2/N_2 and its highly corrosive behavior when exposed to trace water vapor. Our findings here help shape our design of a Li nitride coating on Li metal that greatly improves battery performance, demonstrating the importance of coupling fundamental studies with engineering solutions.

Li Metal Passivation in Dry Oxygen and Nitrogen. Figures 2a and 3a display time-lapse TEM images of the passivation (Figure 2a) and corrosion (Figure 3a) process in

DOI: 10.1021/acs.nanolett.7b02630
Nano Lett. XXXX, XXX, XXX−XXX

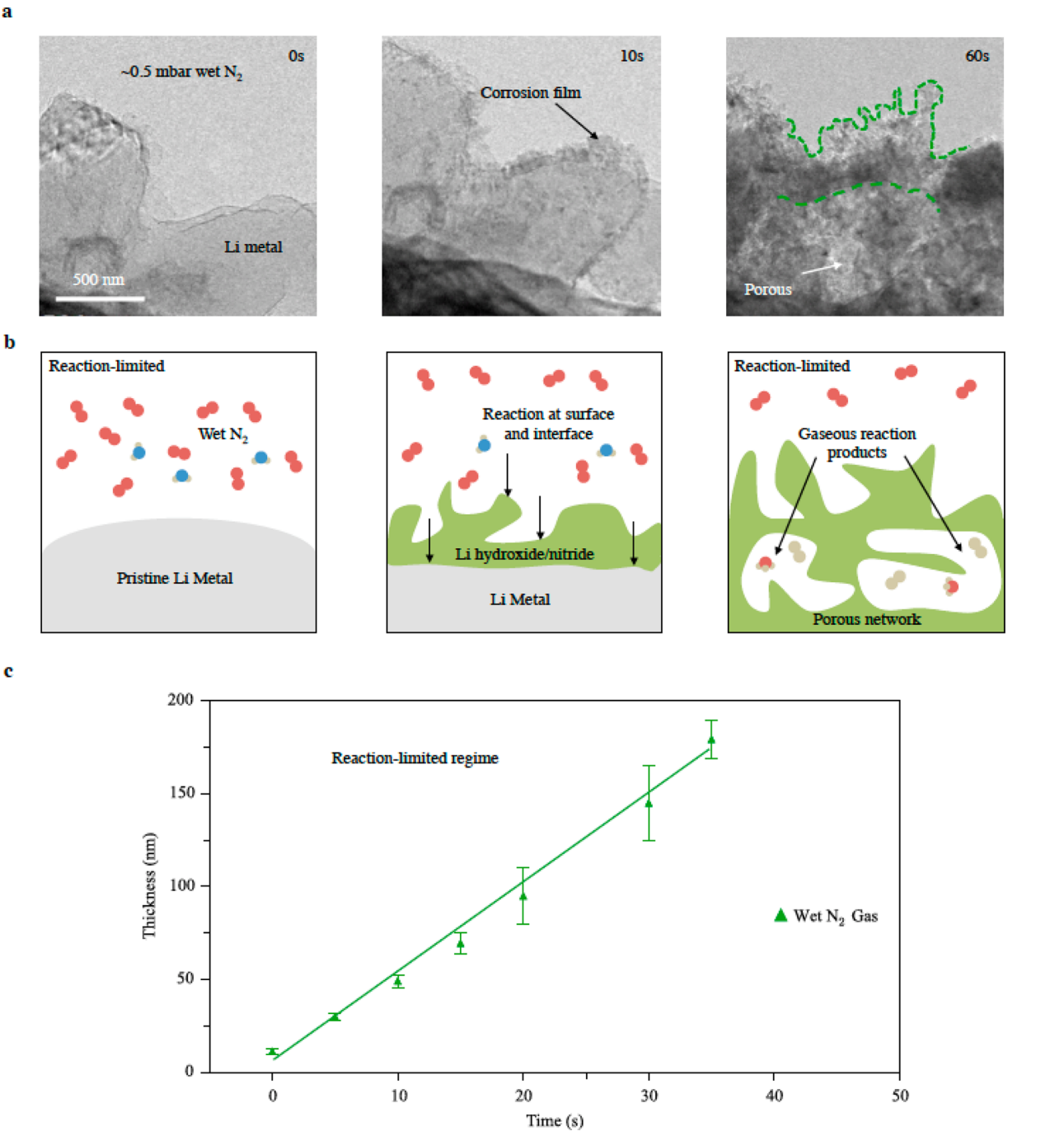

Figure 3. Corrosion and consumption of Li metal in wet N_2 gas. (a) Time-lapse TEM images of Li metal reacting with wet N_2 taken from Movie S2. The pristine Li metal is consumed to form a porous network of corrosion products that grow outward as filaments. (b) Schematic illustrating the corrosion mechanism of Li metal in wet N_2. Since Li nitride is no longer inert in the presence of H_2O, reactions can occur at both the solid−solid and the solid−gas interface. (c) Graph of average corrosion film thickness measured over time. Without a diffusion barrier, the growth rate in wet N_2 is linear and reaction-limited. Guides for the eye are provided as lines through the data points.

dry and wet N_2 environments, respectively. Despite trace moisture (~1 mol %) being the only difference between the dry and wet conditions, the observed reactions and resulting surface morphologies of Li metal are strikingly dissimilar. When Li metal is exposed to dry N_2, a smooth and conformal passivation layer forms on the surface while the overall morphology of the metal is preserved (Figure 2a). In the supporting video, we clearly see that this layer forms uniformly across the exposed Li metal with increasing thickness over time (Movie S1, Supporting Information). EFTEM data suggest that the layer is Li nitride (Figure S5), which appears darker in contrast than pristine Li metal in the TEM because nitrogen has a higher atomic number than Li. Since we monitor the reaction between Li and dry N_2 in real time, we can use this contrast difference to measure and track the passivation layer thickness as the reaction proceeds (Figure S1). By plotting layer thickness over time (Figure 2c), we clearly distinguish two growth modes: a reaction-limited regime and a diffusion-limited regime separated by the vertical dashed line. The growth rate of the passivation layer is represented by the slope of the curve

DOI: 10.1021/acs.nanolett.7b02630
Nano Lett. XXXX, XXX, XXX−XXX

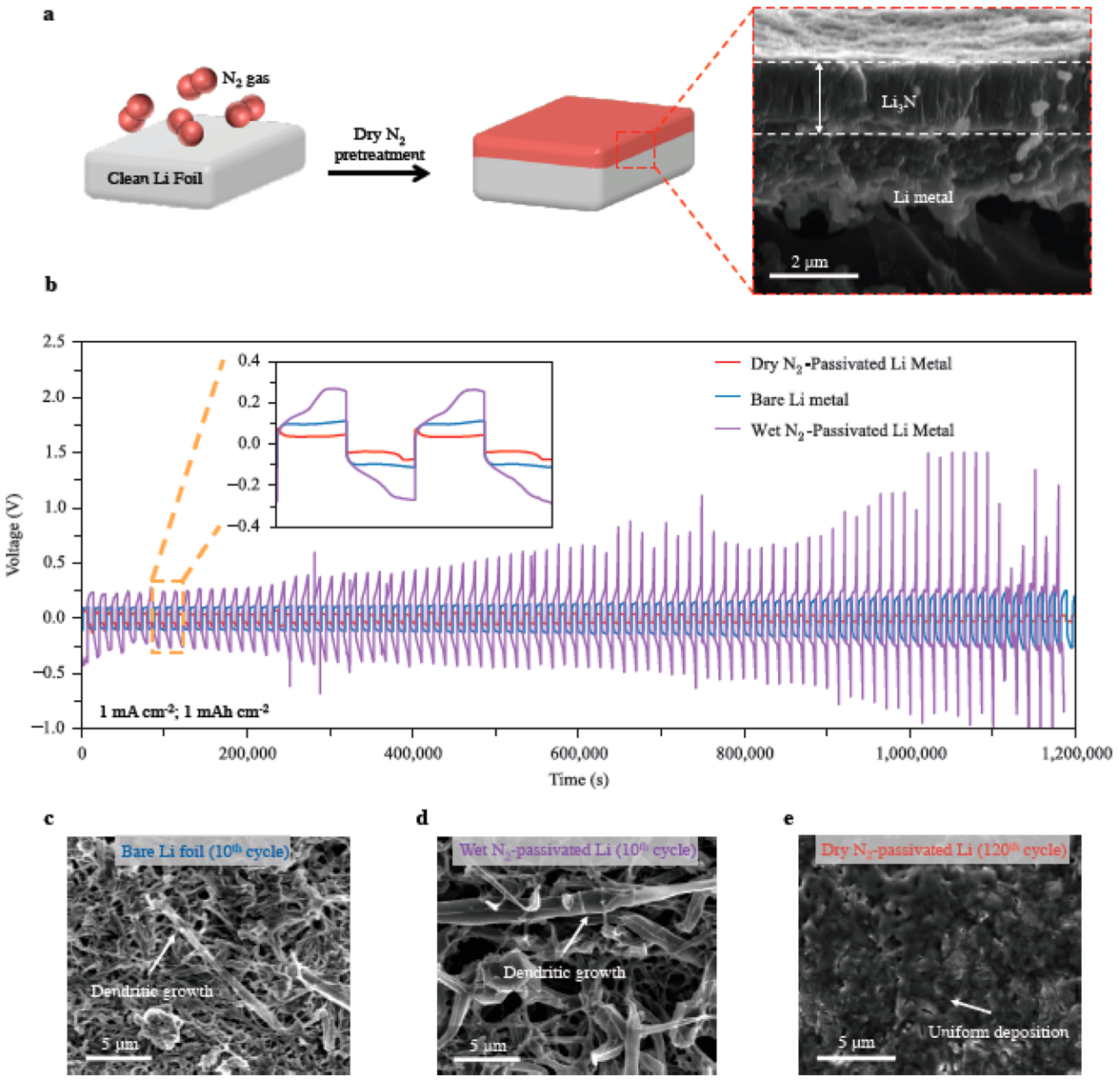

Figure 4. Design and electrochemistry of dry N_2-passivated Li metal anodes. (a) Diagram of the dry N_2 pretreatment on Li metal to form a uniform Li nitride film. The cross-sectional SEM image shows the film is approximately 2 μm. (b) Voltage profiles of bare Li foil, dry N_2-passivated Li foil, and wet N_2-passivated Li foil paired with a pristine Li foil counter electrode. The low overpotential exhibited by the dry N_2-passivated Li foil remains unchanged after 100 cycles in the corrosive carbonate-based electrolyte, suggesting that the SEI formed on the Li nitride layer is stable. Without a protective Li nitride layer, the other samples exhibit large voltage hysteresis that increase over time. (c,d) Top-view SEM image of a bare Li metal foil (c) and a wet N_2-passivated Li metal foil (d) after 10 cycles of Li stripping and deposition (1 mA cm^{-2}, 1 mAh cm^{-2}), showing severe dendrite growth and uneven surface morphology. (e) Top-view SEM image of a dry N_2-passivated Li metal anode after 120 cycles of Li stripping and deposition (1 mA cm^{-2}, 1 mAh cm^{-2}), showing a smooth surface with suppressed dendrite growth.

(Figure 2c), and its reaction mechanism is schematically illustrated in Figure 2b.

Initially, N_2 freely reacts with the clean Li metal surface according to the reaction Li (s) + N_2 (g) → Li_3N (s), rapidly forming a smooth Li nitride layer. Because Li nitride does not react with the surrounding N_2 gas, further reactions must occur at the interface between Li metal and the Li nitride film. During early times (left of the vertical dashed line in Figure 2c), N_2 diffusion through the thin passivation layer is fast and its formation is thus reaction-limited. As the layer grows thicker, it impedes further gas transport to the Li metal and becomes a diffusion barrier for additional reaction. After sufficient time (right of the vertical dashed line in Figure 2c), the passivation layer growth slows down significantly and its formation becomes diffusion-limited. Li metal remains stable after prolonged exposure to N_2 (~5 min), protected from further side reactions by the Li nitride film. We show here that although Li metal has high chemical reactivity, it can be passivated through a self-limiting reaction mechanism that prevents further reaction. The passivation behavior of Li metal in dry N_2 is qualitatively identical to its behavior in dry O_2 (Figures S3, S6; Movie S3) and strongly resembles the oxidation of silicon as described by the Deal-Grove model.[32] However, this model does not hold in wet environments for Li metal as it does for silicon.

Li Metal Corrosion in Trace Moisture Environments. When introduced to wet N_2 containing just ~1 mol % moisture content, Li metal reacts uncontrollably and is quickly consumed despite a shorter exposure time to the surrounding gas (~1 min). The dramatic reaction and change in Li metal

DOI: 10.1021/acs.nanolett.7b02630
Nano Lett. XXXX, XXX, XXX−XXX

morphology is monitored in Movie S2. In stark contrast to its stable passivation in dry environments, Li metal exposed to moisture forms rough and uneven corrosion products that grow outward as filaments until the Li is fully consumed (Figure 3a). After reaction, the original Li metal has degraded into a porous network of these corrosion products. From EFTEM and SAED data, we identify the major corrosion product to be Li hydroxide (Figure S7), which appears darker than Li metal because of the presence of oxygen. Although the corrosion film is not uniform across the entire surface of the Li metal, we can still measure and track the average film thickness over time (Figure 3c). Surprisingly, the growth rate appears linear throughout the reaction and only stops when all the Li is fully depleted. The reaction appears to proceed uninhibited, which is entirely different from the self-limiting growth behavior in dry environments.

To understand this corrosion behavior, we recognize that two gaseous species (N_2 and H_2O) can now react with Li metal. Furthermore, the Li nitride film formed in dry N_2 is no longer inert in the wet gas environment. Thus, in addition to the Li metal reaction with N_2, there are two new reactions that can occur: $2Li\ (s) + 2H_2O\ (g) \rightarrow 2LiOH\ (s) + H_2\ (g)$; $Li_3N\ (s) + 3H_2O\ (g) \rightarrow 3LiOH\ (s) + NH_3\ (g)$. Unlike the passivation reaction that is restricted to the interface between Li nitride and the metal in dry environments, reactions in wet environments can also occur at the interface between the corrosion film and the gas (Figure 3b). As a result, no diffusion barrier exists and the corrosion reactions proceed unimpeded until no Li metal remains. The gas products (H_2 and NH_3) released from these reactions diffuse outward, producing the observed porosity in the final corrosion film. The uneven filamentary growth of the corrosion film may be due to concentration gradients in the gas phase. This phenomenon is similar to dendritic growth observed during battery operation caused by concentration gradients of Li salt in the liquid battery electrolyte. In wet O_2 (Figure S3, Movie S4), Li metal's corrosion behavior is qualitatively identical to the observed behavior in wet N_2. Therefore, we identify H_2O as the primary component that disrupts the passivation of Li metal and elucidate its nanoscale corrosion mechanism.

Electrochemical Performance of Li Metal Passivated by Dry Nitrogen. We can exploit our detailed understanding of these passivation and corrosion reactions to engineer a stable interface on Li metal for improved battery performance. From our operando TEM experiments, we observe that a uniform Li nitride film can be formed on a pristine Li metal surface. Li nitride is known to be a fast ionic conductor[33,34] and can simultaneously serve as a mechanical barrier to reduce dendrite growth, making it a suitable protective layer for Li metal batteries. To form a sufficiently thick Li nitride coating (~2 μm), we carefully clean the surface of a commercial Li foil and then expose the pristine metal to dry N_2 gas prior to battery assembly (Figure 4a). X-ray diffraction data confirm that the nitride passivation layer is crystalline (Figure S8). To evaluate the electrochemical behavior of this Li nitride passivation layer, we constructed 2032 type coin cells (see Methods) with N_2-passivated Li metal as the working electrode and bare Li metal as both the counter and reference electrode. Li with an areal capacity of 1 mAh cm^{-2} was then galvanostatically deposited onto and stripped from the N_2-passivated Li foil at a current density of 1.0 mA cm^{-2}.

Figure 4b shows the voltage profiles of bare Li, dry N_2-passivated Li, and wet N_2-passivated Li as they are cycled over time. After initial formation of the SEI in the first few cycles, the dry N_2-passivated Li foil exhibits low overpotentials of less than 50 mV starting from the 20th cycle. This is due to the fast ionic conductivity of the Li nitride film. The voltage hysteresis remains largely unchanged as the battery is cycled, suggesting that Li nitride stabilizes SEI formation and prevents its cyclic regeneration. By contrast, bare Li foil has a much larger overpotential (100 mV) that increases with cycling, indicating that the SEI is continually being broken/reformed and accumulates on the surface of the Li metal. The voltage profile of the wet N_2-passivated Li is even worse, with overpotentials of over 250 mV that increase dramatically with repeated cycling. From our operando TEM observations, we can explain this large voltage hysteresis by considering the Li hydroxides formed on the Li metal surface during reactions with water. Because Li hydroxide does not conduct Li ions, it only serves as an insulating layer that increases the overpotential needed to electrochemically deposit and strip Li metal. Therefore, it is absolutely critical to minimize moisture in a real battery-processing environment to reduce the formation of these corrosion products on Li metal prior to battery assembly. The electrochemical data here show the importance of reaction conditions in forming a uniform and stable Li nitride layer on Li metal that enables fast kinetics for improved energy efficiency in Li metal batteries.

In addition to energy efficiency, a stable surface morphology during battery cycling is necessary for safe operation. The tendency of Li metal to grow as dendrites during electrochemical deposition presents a major safety concern for battery operation, as these structures can potentially penetrate the polymer separator, causing electrical shorting and thermal runaway.[35] Furthermore, dendrites increase the effective surface area of Li metal, amplifying the consumption of liquid electrolyte and the metal itself through electrochemically driven side reactions. Figure 4c shows a scanning electron microscopy (SEM) image of the bare Li metal surface after 10 cycles in the corrosive carbonate-based electrolytes used in this study. Clearly, erratic dendrite growth dominates the surface, which is detrimental to battery performance and safety. The surface of the wet N_2-passivated Li foil after 10 cycles is also covered with dendrites, as the porous network of Li hydroxide that forms on Li metal does not effectively inhibit dendrite growth (Figure 4d). By contrast, the dry N_2-passived Li foil has a smooth surface even after 120 cycles (Figure 4e, Figure S4). In addition to providing fast transport of Li ions, the uniform Li nitride layer is able to suppress dendrite growth and enable stabilized Li metal batteries. The results presented here represent a simple but telling demonstration of the practical applications that can be initiated by our fundamental gas study on reactive battery materials, opening up many excellent opportunities for scientific discovery and invention.

Methods. *Generating Pristine Li Metal and Operando TEM of Gas Reactions.* During its transfer from an argon glovebox to the environmental transmission electron microscope (ETEM), Li metal will tarnish and form a corrosion layer due to ambient air exposure. To generate pristine Li metal inside the ETEM, we used a specialized dual-probe TEM holder (Nanofactory Instruments AB) capable of spatial manipulation and electrical biasing. One probe was a Cu wire with a diameter of ~0.25 mm and length of ~0.5 cm. The other probe was a W wire with the same dimensions. We physically scratched the surface of Li foil with the W probe to load Li metal onto the tip. The two probes were then secured to the

DOI: 10.1021/acs.nanolett.7b02630
Nano Lett. XXXX, XXX, XXX−XXX

TEM holder and transferred to the ETEM facility in a sealed, airtight container. During insertion into the ETEM, the Li metal on the W tip tarnished from the brief air exposure (~3 s). This tarnish layer consisted of oxides and nitrides that act as a solid electrolyte, permitting the flow of Li ions during electrical biasing. All experiments were carried out using a FEI Titan 80-300 ETEM operated at 300 kV. The microscope was equipped with an aberration corrector in the image forming (objective lens) and a Gatan 966 Quantum electron energy loss (EEL) spectrometer.

Once the TEM holder was fully inserted, the Cu and W probes were brought into physical contact by manipulating the piezoelectric controller. Fresh Li metal with a clean surface was then plated onto the Cu wire by applying a negative bias of −3 V. After sufficient Li metal was plated (~5−10 min), we introduced gas at a pressure of ~0.5 mbar into the ETEM and observed the reaction with Li metal in real time. The pressure in the microscope chamber was monitored using an Edwards Barocell 600 capacitance manometer, with a precision of ±3%. In order to avoid condensation of contaminants on the Li metal during gas flow, we used a liquid nitrogen-cooled coldfinger next to our sample. After the passivation/corrosion reaction was complete, the gas was pumped out of the ETEM, and EEL spectra of the corrosion film and Li metal were collected.

Electrochemical Characterization. In an argon-filled glovebox, bare Li metal and N_2-passivated Li metal working electrodes were assembled into type 2032 coin cells with a polymer separator (Celgard 2250) and bare Li metal (Alfa Aesar) as the counter/reference electrode. 50 μL of 1.0 M $LiPF_6$ in 1:1 v/v ethylene carbonate/diethyl carbonate (BASF Selectilyte LP40) was added as the electrolyte with full wetting of both working and counter electrode surfaces. Coin cells were loaded into a battery tester (Arbin Instruments) and cycled with an areal capacity of 1 mAh cm^{-2} at a current density of 1.0 mA cm^{-2}. For *ex situ* scanning electron microscopy (SEM) characterization of working electrodes, coin cells were disassembled, and the working electrodes were then rinsed gently in 1,3-Dioxolane (DOL) to remove Li salts from the residual electrolyte. The cleaned samples were then transferred out of the glovebox in an airtight container to the SEM facility. SEM images were taken on a FEI Sirion and Nova NanoSEM.

Thickness Measurement of Passivation and Corrosion film. To plot the thickness of the passivation and corrosion layers over time, we took still frames of the Li metal morphology at specific time points. We distinguish the pure Li metal from the passivation/corrosion film by the difference in contrast of the high resolution TEM image. The thickness can then be measured at multiple points by using ImageJ software. An example for the dry oxygen case is given in Figure S1. Using ImageJ software, we drew a straight line and overlaid it on the bottom-left scale bar. Then, going to "Analyze" → "Set Scale···" we could define the length (200 nm) of this straight line. In this way, any line subsequently drawn will be scaled accordingly. The red circles in Figure S1 denote the five regions where we measured the Li oxide thickness. Averaging these values gives us the mean and standard deviation, which can be plotted as a function of time.

■ ASSOCIATED CONTENT

Supporting Information

The Supporting Information is available free of charge on the ACS Publications website at DOI: 10.1021/acs.nanolett.7b02630.

Experimental details, additional figures (PDF)

Clean Li metal surface reacting with dry nitrogen gas (AVI)

Clean Li metal surface reacting with wet nitrogen gas (AVI)

Clean Li metal surface reacting with dry oxygen gas (AVI)

Clean Li metal surface reacting with wet oxygen gas (AVI)

■ AUTHOR INFORMATION

Corresponding Author

*E-mail: yicui@stanford.edu.

ORCID

Yuzhang Li: 0000-0002-1502-7869

Ai Leen Koh: 0000-0003-1991-100X

Allen Pei: 0000-0001-8930-2125

Author Contributions

⊥Yuzhang Li and Yanbin Li contributed equally to this work. Yuzhang Li, Yanbin Li, and Y.C. conceived and designed the experiments. Yuzhang Li and A.L.K. conducted environmental TEM characterization. Yanbin Li and Y.S. carried out materials synthesis and electrochemical characterization. Yuzhang Li and B.B. performed EFTEM and SAED characterization. K.Y., J.Z., and A.P. worked on other characterizations. Yuzhang Li, Yanbin Li, and Y.C. cowrote the paper. All authors discussed the results and commented on the manuscript.

Notes

The authors declare no competing financial interest.

■ ACKNOWLEDGMENTS

Yuzhang Li acknowledges the National Science Foundation Graduate Research Fellowship Program (NSF GRFP) for funding. A.P. acknowledges the support from the U.S. Department of Defense through the National Defense Science & Engineering Graduate Fellowship (NDSEG) Program and from Stanford University through the Stanford Graduate Fellowship (SGF) Program. B.B. (particularly) acknowledges financial support by the German Research Foundation (DFG) under Grant No. BU 2875/2-1. Y.C. acknowledges the support from the Assistant Secretary for Energy Efficiency and Renewable Energy, Office of Vehicle Technologies of the U.S. Department of Energy under the Battery Materials Research (BMR) Program and Battery 500 Consortium Programs.

■ REFERENCES

(1) Chu, S.; Majumdar, A. *Nature* **2012**, *488* (7411), 294−303.

(2) Huang, J. Y.; Zhong, L.; Wang, C. M.; Sullivan, J. P.; Xu, W.; Zhang, L. Q.; Mao, S. X.; Hudak, N. S.; Liu, X. H.; Subramanian, A.; et al. *Science* **2010**, *330* (6010), 1515−1520.

(3) McDowell, M. T.; Lee, S. W.; Harris, J. T.; Korgel, B. A.; Wang, C.; Nix, W. D.; Cui, Y. *Nano Lett.* **2013**, *13* (2), 758−764.

(4) Gu, M.; Parent, L. R.; Mehdi, B. L.; Unocic, R. R.; McDowell, M. T.; Sacci, R. L.; Xu, W.; Connell, J. G.; Xu, P.; Abellan, P.; et al. *Nano Lett.* **2013**, *13* (12), 6106−6112.

(5) Weker, J. N.; Liu, N.; Misra, S.; Andrews, J. C.; Cui, Y.; Toney, M. F. *Energy Environ. Sci.* **2014**, *7* (8), 2771−2777.

(6) Lim, J.; Li, Y.; Alsem, D. H.; So, H.; Lee, S. C.; Bai, P.; Cogswell, D. A.; Liu, X.; Jin, N.; Yu, Y.; et al. *Science* **2016**, *353* (6299), 566−571.

(7) Bañares, M. A. *Adv. Mater.* **2011**, *23* (44), 5293−5301.

DOI: 10.1021/acs.nanolett.7b02630
Nano Lett. XXXX, XXX, XXX−XXX

(8) Sanchez Casalongue, H. G.; Ng, M. L.; Kaya, S.; Friebel, D.; Ogasawara, H.; Nilsson, A. *Angew. Chem., Int. Ed.* **2014**, *53* (28), 7169−7172.
(9) Zheng, H.; Smith, R. K.; Jun, Y.; Kisielowski, C.; Dahmen, U.; Alivisatos, A. P. *Science* **2009**, *324* (5932), 1309−1312.
(10) Zheng, H.; Rivest, J. B.; Miller, T. A.; Sadtler, B.; Lindenberg, A.; Toney, M. F.; Wang, L.-W.; Kisielowski, C.; Alivisatos, A. P. *Science* **2011**, *333* (6039), 206−209.
(11) Markowitz, M. M.; Boryta, D. A. *J. Chem. Eng. Data* **1962**, *7* (4), 586−591.
(12) U.S. Department of Energy; Jeppson, D. W. *Lithium literature review: lithium's properties and interactions*; Department of Energy: Washington, DC, 1978.
(13) Bruce, P. G.; Freunberger, S. A.; Hardwick, L. J.; Tarascon, J.-M. *Nat. Mater.* **2012**, *11* (1), 19−29.
(14) Xu, W.; Wang, J.; Ding, F.; Chen, X.; Nasybulin, E.; Zhang, Y.; Zhang, J.-G. *Energy Environ. Sci.* **2014**, *7* (2), 513−537.
(15) Aurbach, D.; Zinigrad, E.; Cohen, Y.; Teller, H. *Solid State Ionics* **2002**, *148* (3), 405−416.
(16) Xu, K. *Chem. Rev.* **2004**, *104* (10), 4303−4418.
(17) Brissot, C.; Rosso, M.; Chazalviel, J.-N.; Lascaud, S. *J. Power Sources* **1999**, *81*, 925−929.
(18) Kamaya, N.; Homma, K.; Yamakawa, Y.; Hirayama, M.; Kanno, R.; Yonemura, M.; Kamiyama, T.; Kato, Y.; Hama, S.; Kawamoto, K.; et al. *Nat. Mater.* **2011**, *10* (9), 682−686.
(19) Bouchet, R.; Maria, S.; Meziane, R.; Aboulaich, A.; Lienafa, L.; Bonnet, J.-P.; Phan, T. N. T.; Bertin, D.; Gigmes, D.; Devaux, D.; et al. *Nat. Mater.* **2013**, *12* (5), 452−457.
(20) Ding, F.; Xu, W.; Graff, G. L.; Zhang, J.; Sushko, M. L.; Chen, X.; Shao, Y.; Engelhard, M. H.; Nie, Z.; Xiao, J.; et al. *J. Am. Chem. Soc.* **2013**, *135* (11), 4450−4456.
(21) Zheng, G.; Lee, S. W.; Liang, Z.; Lee, H.-W.; Yan, K.; Yao, H.; Wang, H.; Li, W.; Chu, S.; Cui, Y. *Nat. Nanotechnol.* **2014**, *9* (8), 618−623.
(22) Yan, K.; Lee, H.-W.; Gao, T.; Zheng, G.; Yao, H.; Wang, H.; Lu, Z.; Zhou, Y.; Liang, Z.; Liu, Z.; Chu, S.; Cui, Y. *Nano Lett.* **2014**, *14* (10), 6016−6022.
(23) Li, W.; Yao, H.; Yan, K.; Zheng, G.; Liang, Z.; Chiang, Y.-M.; Cui, Y. *Nat. Commun.* **2015**, *6*, 7436.
(24) Qian, J.; Henderson, W. A.; Xu, W.; Bhattacharya, P.; Engelhard, M.; Borodin, O.; Zhang, J.-G. *Nat. Commun.* **2015**, *6*, 6362.
(25) Yan, K.; Lu, Z.; Lee, H.-W.; Xiong, F.; Hsu, P.-C.; Li, Y.; Zhao, J.; Chu, S.; Cui, Y. *Nat. Energy* **2016**, *1*, 16010.
(26) Liang, Z.; Lin, D.; Zhao, J.; Lu, Z.; Liu, Y.; Liu, C.; Lu, Y.; Wang, H.; Yan, K.; Tao, X.; et al. *Proc. Natl. Acad. Sci. U. S. A.* **2016**, *113* (11), 2862−2867.
(27) Liu, Y.; Lin, D.; Liang, Z.; Zhao, J.; Yan, K.; Cui, Y. *Nat. Commun.* **2016**, *7*, 10992.
(28) Lin, D.; Liu, Y.; Liang, Z.; Lee, H.-W.; Sun, J.; Wang, H.; Yan, K.; Xie, J.; Cui, Y. *Nat. Nanotechnol.* **2016**, *11*, 626−632.
(29) Grady, H. R. *J. Power Sources* **1980**, *5* (1), 127−135.
(30) Zhao, J.; Lu, Z.; Liu, N.; Lee, H.-W.; McDowell, M. T.; Cui, Y. *Nat. Commun.* **2014**, *5*, 5088.
(31) Zhao, J.; Lee, H.-W.; Sun, J.; Yan, K.; Liu, Y.; Liu, W.; Lu, Z.; Lin, D.; Zhou, G.; Cui, Y. *Proc. Natl. Acad. Sci. U. S. A.* **2016**, *113*, 7408−7413.
(32) Deal, B. E.; Grove, A. S. *J. Appl. Phys.* **1965**, *36* (12), 3770−3778.
(33) Boukamp, B. A.; Huggins, R. A. *Phys. Lett. A* **1976**, *58* (4), 231−233.
(34) Boukamp, B. A.; Huggins, R. A. *Mater. Res. Bull.* **1978**, *13* (1), 23−32.
(35) Wang, Q.; Ping, P.; Zhao, X.; Chu, G.; Sun, J.; Chen, C. *J. Power Sources* **2012**, *208*, 210−224.

DOI: 10.1021/acs.nanolett.7b02630
Nano Lett. XXXX, XXX, XXX−XXX